International Journal for Modern Trends in Science and Technology
Volume 12, Issue 07, pages 109-122.
ISSN: 2455-3778 online
Available online at: http://www.ijmtst.com/vol12issue06.html
DOI: https://doi.org/10.5281/zenodo.20739610

Adaptive Intelligent Model Predictive Control for Power Quality Enhancement and System Stability in Solar PV Assisted Zeta Converter Based Bidirectional EV Charging Stations

Shreema[1] | M. Harish[2] | Dr. K. Siva Kumar[3]

[1]*PG Student, Dept. of Electrical & Electronics Engineering, Sri Venkatesa Perumal College of Engineering and Technology, Puttur, Andhra Pradesh, India*
[2]*Assistant Professor, Dept. of Electrical & Electronics Engineering, Sri Venkatesa Perumal College of Engineering and Technology, Puttur, Andhra Pradesh, India*
[3]*Professor, Dept. of Electrical & Electronics Engineering, Sri Venkatesa Perumal College of Engineering and Technology, Puttur, Andhra Pradesh, India*

To Cite this Article
Shreema, M. Harish & Dr. K. Siva Kumar (2026). Adaptive Intelligent Model Predictive Control for Power Quality Enhancement and System Stability in Solar PV Assisted Zeta Converter Based Bidirectional EV Charging Stations. International Journal for Modern Trends in Science and Technology, 12(07), 109-122. https://doi.org/10.5281/zenodo.20739610

Article Info
Received: 05 June 2026; Revised: 05 July 2026; Accepted: 08 July 2026.

KEYWORDS

Artificial Neural Network (ANN), Model Predictive Control (MPC), Solar Photovoltaic (PV), Bidirectional DC–DC Zeta Converter, Bidirectional EV Charging Station, Grid-to-Vehicle (G2V), Vehicle-to-Grid (V2G), Power Quality Enhancement, DC-Link Voltage Regulation, Maximum Power Point Tracking (MPPT).

ABSTRACT

Adaptive Artificial Neural Network (ANN)-based Model Predictive Control (MPC) is proposed for a grid-connected solar PV-assisted bidirectional electric vehicle (EV) charging station to improve system stability, power quality, and energy management during G2V and V2G operations. A solar PV source and a bidirectional DC–DC Zeta converter effectively transmit power between the PV array, EV battery, and utility grid, reducing grid reliance and ensuring a reliable power supply. Minimal switching losses, excellent conversion efficiency, continuous input and output current, and fast charging and discharging characterize the bidirectional Zeta converter. To overcome the limitations of DC-link voltage and dq-axis voltage-current control under dynamic operating conditions, an adaptive ANN controller with Model Predictive Control (MPC) is developed for real-time prediction and optimal converter switching state selection. To minimize transient oscillations, voltage fluctuations, and dynamic disturbances during sudden load changes, solar irradiance variations, and seamless transitions between G2V and V2G operating modes, the ANN continuously adjusts controller parameters to regulate DC-link voltage, grid frequency, and bidirectional power Voltage distortion, current harmonics, reactive power fluctuations, and frequency variations are reduced via grid-side compensation, *improving power quality and system stability. Under different operating situations, MATLAB/Simulink models and validates the system. While meeting IEEE 519 Total Harmonic Distortion (THD) restrictions, simulations indicate enhanced DC-link voltage control, grid frequency stability, transient responsiveness, dynamic oscillations, converter efficiency, and solar energy use Solar PV-assisted bidirectional EV charging stations can benefit from the adaptive ANN–MPC control strategy's improved DC-link voltage regulation, grid frequency stability, power quality, and utility grid dependence.*

1. INTRODUCTION

Due to global need for clean energy and sustainable transportation, electric vehicles (EVs) are being adopted rapidly as an effective alternative to internal combustion engine automobiles. Growing worries about greenhouse gas emissions, climate change, fossil fuel depletion, and strict environmental restrictions have spurred governments and industry worldwide to promote electric mobility and renewable energy-based transportation systems [1], [2]. The transportation sector accounts for a large amount of global carbon emissions and energy consumption, making EV adoption crucial for carbon neutrality and sustainable development. Thus, efficient, dependable, and intelligent EV charging infrastructure is a top smart grid research priority [3]. Existing electrical power systems face many technological hurdles as EV penetration rises. Massive EV charging increases electricity consumption, causing peak loads transformer overloading, feeder congestion, voltage variations, frequency deviations, network losses, and power quality degradation [4]. Urban distribution networks with several fast-charging stations and highly dynamic charging circumstances make these difficulties worse. EV users' stochastic charging behavior increases power demand unpredictability, making energy scheduling and grid management harder. Therefore, improved charging station architectures with intelligent power management and dynamic grid assistance are necessary for power system reliability [5]. To charge EV batteries, Grid-to-Vehicle (G2V) charging stations exclusively need utility grid electricity. This method charges EV batteries easily but does not completely utilize their energy storage capacity. Due to advances in bidirectional charging technology, electric vehicles may now discharge stored energy back to the utility grid when electricity is needed [6]. This bidirectional power exchange turns EV batteries into distributed energy storage systems for peak load reduction, frequency regulation, voltage stability, renewable energy balancing, emergency backup power, spinning reserve, and auxiliary grid services [7]. Thus, bidirectional EV charging stations are essential to future smart grids because they promote energy flexibility, system resilience, and renewable energy use [8]. Despite these benefits, bidirectional EV charging stations provide converter control, battery management, renewable energy unpredictability, and power quality difficulties. Sudden load changes, nonlinear converter dynamics, battery parameter uncertainties, quick G2V-V2G mode transitions, and fluctuating renewable energy generation might influence converter performance and system stability during charging and discharging [9]. Dynamic operating conditions because voltage oscillations, current distortion, switching losses, reactive power fluctuations, and converter efficiency loss. For modern EV charging infrastructures, developing intelligent converter control techniques that can adapt to changing operating conditions is a research priority [10]. Renewable energy sources at EV charging stations minimize dependence on conventional utility generation and improve environmental sustainability, attracting attention. Solar photovoltaic (PV) systems are one of the most promising renewable energy sources due to their abundance, modular construction, low maintenance, silent operation, and reducing installation prices [11]. Solar PV-assisted EV charging stations employ renewable energy to charge batteries, decreasing grid electricity and greenhouse gas emissions. Photovoltaic power generation is strongly reliant on solar irradiation and ambient temperature, generating output voltage and power fluctuations. These intermittent properties make converter operation and power exchange between the PV array, EV battery, and utility grid more difficult [12]. Power electronic converters are essential in renewable energy-assisted EV charging systems for effective energy conversion under various conditions. Various bidirectional DC-DC converter topologies, including as buck-boost, Ćuk, SEPIC, flyback, DAB, and isolated converters, have been studied for EV charging [13]. The bidirectional Zeta converter is popular due to its high voltage conversion capability, continuous input and output current characteristics, reduced current ripple, low switching stress, high voltage gain, and improved conversion efficiency [14]. The Zeta converter converts voltage step-up and step-down without inverting output voltage, unlike buck–boost converters. Continuous charging reduces current ripple, extends battery life, and boosts charging efficiency. The Zeta converter is ideal for high-power bidirectional EV charging stations with dynamic loading due to its low conduction losses and fast transient response [15]. Advanced converter topologies improve energy conversion efficiency; yet efficient power transfer between renewable energy sources, EV batteries, and utility grids is difficult. Due to high-frequency switching operations and nonlinear converter behavior, grid-connected charging stations induce harmonic distortion, reactive power fluctuations, voltage sag, voltage swell, frequency deviations, electromagnetic interference, and power factor degradation [16]. Converter dependability, transformer performance, battery charging efficiency, and sensitive electrical equipment connected to the same distribution network are affected by poor power quality. Modern EV charging stations must meet tight international standards like IEEE 519 and IEEE 1547 by ensuring minimal THD, steady voltage profiles, sinusoidal grid current, and near-unity power factor [17]. EV charging systems have traditionally used proportional-integral (PI) controllers and dq-axis voltage-current control techniques to regulate DC-link voltage, converter current, and bidirectional power flow [18]. Three-phase electrical quantities are converted into rotating reference frame components using dq-axis control, allowing active and reactive power regulation. These controllers function well and are easy to implement under balanced steady-state conditions. Conventional controllers generally reduce dynamic performance due to rapid solar irradiation changes, unexpected charging demand, converter nonlinearities, parameter uncertainties, and frequent G2V-V2G transitions [19]. Their constant controller gains cannot compensate for changing operating conditions, causing overshoot, extended settling time, oscillatory response, current distortion, and poor disturbance rejection [20]. Model Predictive Control (MPC) can predict system behavior and calculate optimal converter switching states using a specified optimization cost function, making it one of the most powerful advanced control approaches for power electronic converters [21]. MPC directly controls converter switching without pulse-width modulation or stacked control loops, unlike cascaded PI controllers. The predictive controller evaluates converter voltage and current responses for all switching states at each sample interval and chooses the switching sequence that minimizes prediction error while fulfilling converter restrictions. Therefore, MPC offers faster transient response, better current tracking accuracy, lower overshoot, better disturbance rejection, and effective multivariable control under rapidly changing operating conditions [22].

MPC outperforms conventional controllers, although its success depends on the mathematical converter model's accuracy and the optimization function's weighting parameters. Converter parameter fluctuations, battery aging, thermal impacts, renewable energy intermittency, and modeling uncertainties can lower controller performance and prediction accuracy [23]. Engineering expertise and offline tweaking are needed to choose weighting coefficients for varied operating situations. These constraints spur the development of adaptive intelligent control methods that update controller parameters in real time. Recent advances in artificial intelligence offer a promising alternative to predictive control. Artificial Neural Networks (ANNs) excel at nonlinear system identification, adaptive learning, prediction, optimization, and intelligent decision-making [24]. ANN controllers learn converter characteristics from measured operation data and automatically adjust controller parameters to changing environmental circumstances. Their capacity to approximate complex nonlinear interactions without correct mathematical models improves controller robustness under unknown operating conditions. Adaptive ANN methods improve prediction accuracy, converter switching decisions, parameter changes, and system stability during dynamic charging and discharging when coupled with Model Predictive Control [25]. Considering these problems, this study presents an AI–MPC technique for a solar PV-assisted bidirectional EV charging station using a bidirectional DC–DC Zeta converter. The suggested controller uses Model Predictive Control's quick prediction and adaptive intelligent learning to pick converter switching states accurately under different operating conditions. In Grid-to-Vehicle (G2V) and Vehicle-to-Grid (V2G) operating modes, the intelligent controller continuously regulates DC-link voltage, controls bidirectional power flow, suppresses voltage fluctuations, minimizes current harmonics, reduces converter switching losses, and improves power quality. An effective grid-side compensation method reduces reactive power oscillations, voltage distortion, frequency deviations, and transient disturbances, meeting IEEE 519 and IEEE 1547 standards. The full solar PV-assisted EV charging system is modeled in MATLAB/Simulink and tested under unexpected load variations, rapid solar irradiance changes, charging-to-discharging transitions, and dynamic grid disruptions. Compared to conventional DC-link voltage and dq-axis voltage-current control strategies, the simulation results show significant improvements in DC-link voltage regulation, converter efficiency, transient response, harmonic mitigation, renewable energy utilization, and system stability.

The major contributions of this work are summarized as follows:

- Development of a grid-connected solar PV-assisted bidirectional EV charging station using a bidirectional DC–DC Zeta converter.
- Design of an Adaptive Intelligent Model Predictive Control strategy for optimal converter switching and energy management.
- Accurate regulation of DC-link voltage and bidirectional power flow during both G2V and V2G operation.
- Fast transient response and improved stability under rapid solar irradiance variations and sudden load disturbances.
- Effective reduction of voltage distortion, current harmonics, reactive power oscillations, and frequency deviations.
- Enhanced converter efficiency with reduced switching and conduction losses.
- Improved utilization of solar PV energy while reducing dependence on the utility grid.

II. SYSTEM CONFIGURATION

The proposed system consists of a solar photovoltaic (PV) array, a bidirectional DC–DC Zeta converter, an electric vehicle (EV) battery, a DC-link capacitor, a three-phase Voltage Source Converter (VSC), a utility grid, and an Adaptive Artificial Neural Network (ANN)-based Model Predictive Control (MPC) unit as shown in Fig.1. The solar PV array serves as the primary renewable energy source and supplies power to the EV charging station while reducing dependence on the utility grid. The bidirectional Zeta converter enables efficient power transfer between the PV system, EV battery, and DC-link during both Grid-to-Vehicle (G2V) and Vehicle-to-Grid (V2G) operations. During G2V mode, power is delivered from the PV array and utility grid to charge the EV battery. During V2G mode, the stored battery energy is supplied back to the utility grid to support grid demand and improve energy utilization. The Adaptive ANN-based MPC continuously predicts system behavior and selects the optimal converter switching state to regulate the DC-link voltage, control bidirectional power flow, and minimize voltage fluctuations, current harmonics, and switching losses. A grid-side Voltage Source Converter maintains synchronization with the utility grid and improves power quality by reducing reactive power variations and Total Harmonic Distortion (THD). The complete system is implemented in MATLAB/Simulink to evaluate its performance under varying solar irradiance, load disturbances, and G2V/V2G operating conditions. The proposed configuration provides improved converter efficiency, enhanced system stability, effective power quality enhancement, and better utilization of renewable energy while satisfying IEEE 519 and IEEE 1547 standards.

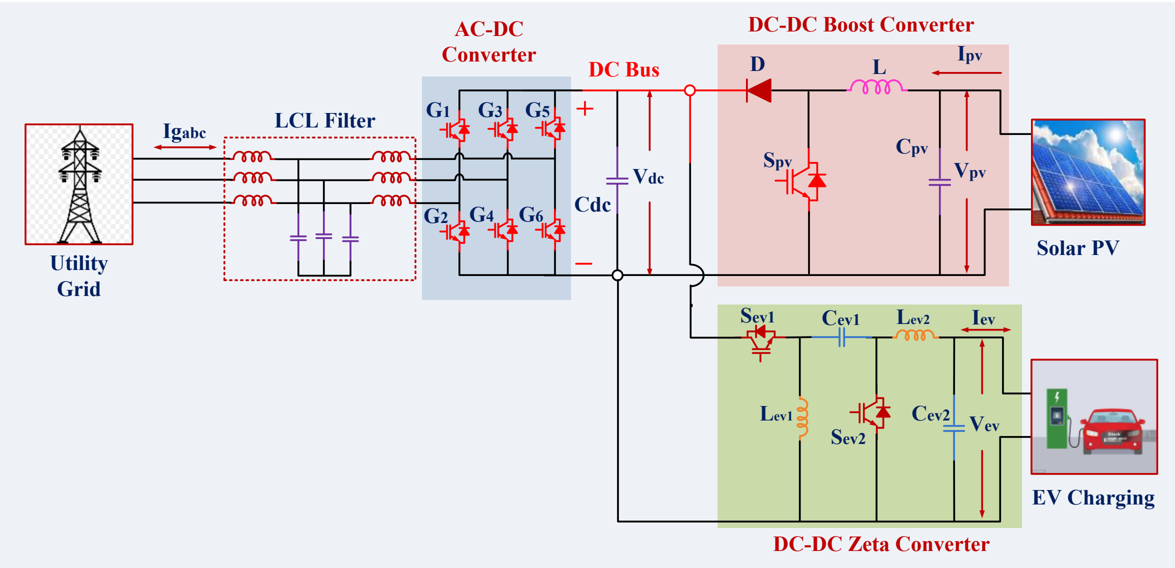

Fig. 1 Proposed System Configuration of the Solar PV-Connected Bidirectional EV Charging Station Using a Bidirectional Zeta Converter

III. SOLAR PV SYSTEM

A. Solar PV Configuration with P&O MPPT

The proposed solar photovoltaic (PV) subsystem serves as the primary renewable energy source for the bidirectional EV charging station. It consists of a photovoltaic array, a DC–DC boost converter, and a Perturb and Observe (P&O)-based Maximum Power Point Tracking (MPPT) controller as shown in Fig.2. The PV array converts solar irradiance into DC electrical power, while the boost converter regulates the output voltage and transfers the maximum available solar energy to the common DC-link. Since the output characteristics of the PV array vary continuously with changes in solar irradiance and cell temperature, the P&O MPPT algorithm is employed to continuously track the maximum power point (MPP), thereby maximizing energy extraction and improving the overall efficiency of the charging station. The generated PV voltage and current are measured continuously by the MPPT controller. Based on the measured power variation, the controller adjusts the duty cycle of the boost converter to force the PV array to operate at its maximum power point. Consequently, the proposed configuration provides stable DC-link voltage, improved renewable energy utilization, and enhanced charging performance under varying environmental conditions.

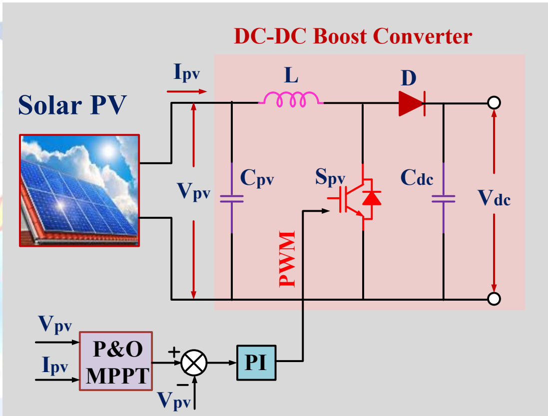

Fig. 2 Solar PV System with P&O MPPT

B. Solar PV Mathematical Model

The output current of a photovoltaic cell is expressed as

$$I = I_{Ph} - I_o\left(e^{\frac{q(V+IR_S)}{nkT}} - 1\right) - \frac{V+IR_S}{R_{sh}} \quad (1)$$

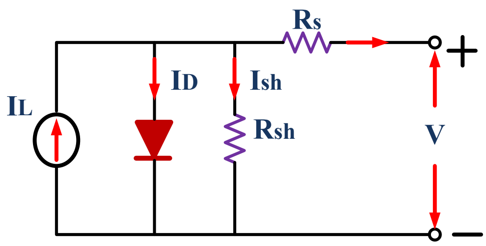

Fig. 3 equivalent model of PV solar.

Where

- I_{PV} = PV output current(A)
- I_{Ph} = Photocurrent(A)
- I_o = Diode saturation current(A)
- R_s = Series resistance(ohms)
- R_{sh} = Shunt resistance(ohms)
- q = Electron charge
- k = Boltzmann constant

- T = Cell temperature(K)
- n = Diode ideality factor

The output power generated by the PV array is

$$P_{PV} = V_{PV} \cdot I_{PV} \tag{2}$$

The maximum power point occurs when

$$V_{out} = \frac{V_{in}}{1-D} \tag{3}$$

C. DC–DC Boost Converter

The dynamic behavior of the DC–DC boost converter can be accurately represented using a state-space model. This mathematical model describes the variation of the converter state variables with respect to time and is widely used for controller design, stability analysis, and dynamic performance evaluation. In the proposed solar PV-assisted EV charging station, the boost converter operates in continuous conduction mode (CCM), where the inductor current never reaches zero during a switching cycle. The converter has two operating states depending on the switching position of the power semiconductor switch. The state variables selected for modeling are the inductor current and the output capacitor voltage because they represent the energy stored in the magnetic and electric fields of the converter. The state variables are defined as

$$x_1 = i_L \tag{4}$$

$$x_2 = V_{dc} \tag{5}$$

where

- i_L = Inductor current (A)
- V_{dc} = Output DC-link voltage (V)

Mode 1: Switch ON (S = ON)

When the power switch is turned ON, the input source is directly connected to the inductor. During this interval, the inductor stores energy supplied by the photovoltaic array, while the diode becomes reverse biased and isolates the output side from the input. Consequently, the load is supplied only by the output capacitor. The inductor current increases linearly because the full PV voltage appears across the inductor, whereas the capacitor voltage gradually decreases as it discharges through the load resistance.

Applying Kirchhoff's Voltage Law (KVL) to the inductor loop gives

$$\frac{di_L}{dt} = \frac{V_{pv}}{L} \tag{6}$$

Applying Kirchhoff's Current Law (KCL) at the output capacitor,

$$C\frac{dV_{dc}}{dt} = -\frac{V_{dc}}{R} \tag{7}$$

Where

- L = Boost inductor
- C = Output capacitor
- R = Load resistance

During this interval, energy is accumulated in the inductor, preparing it for transfer to the output during the OFF state.

Mode 2: Switch OFF (S = OFF)

When the power switch is turned OFF, the stored magnetic energy in the inductor is released through the diode to the output capacitor and load. As a result, both the photovoltaic source and the inductor simultaneously deliver power to the output. This operating mode is responsible for boosting the input voltage to a higher DC-link voltage.

Applying KVL gives

$$\frac{di_L}{dt} = \frac{V_{pv}-V_{dc}}{L} \tag{8}$$

Similarly, applying KCL at the output capacitor yields

$$\frac{dV_{dc}}{dt} = \frac{i_L}{C} - \frac{V_{dc}}{RC} \tag{9}$$

During this interval, the inductor transfers its stored energy to the capacitor and load, causing the output voltage to increase above the input PV voltage.

Since the boost converter repeatedly switches between the ON and OFF states within every switching period, the overall converter dynamics can be represented using an averaged state-space model. The averaging process combines both operating modes according to the duty cycle D, where D represents the fraction of one switching period during which the switch remains ON.

The averaged inductor current equation becomes

$$\frac{di_L}{dt} = \frac{V_{pv}-(1-D)V_{dc}}{L} \tag{10}$$

Similarly, the averaged capacitor voltage equation is

$$\frac{dV_{dc}}{dt} = \frac{(1-D)i_L}{c} - \frac{V_{dc}}{Rc} \tag{11}$$

where

- D = Duty cycle
- 0≤D≤1

These equations describe the complete dynamic behavior of the boost converter under continuous conduction mode.

D. Perturb and Observe (P&O) MPPT Algorithm

The Perturb and Observe (P&O) algorithm is a simple and widely used Maximum Power Point Tracking (MPPT) technique for photovoltaic (PV) systems as shown in Fig.2. Its objective is to continuously extract the maximum available power from the PV array under varying solar irradiance and temperature conditions. The controller periodically measures the PV voltage (V_{pv}) and current (Ipv) to calculate the output power as

$$P(k) = V_{PV}(k) \times I_{PV}(k) \quad (12)$$

The changes in power and voltage are determined by

$$\Delta P = P(k) - P(k-1) \quad (13)$$

$$\Delta V = V_{Pv}(k) - V_{pv}(k-1) \quad (14)$$

If the power increases (ΔP>0), the controller continues perturbing the operating point in the same direction. If the power decreases (ΔP<0), the perturbation direction is reversed as shown in Fig.4. Based on this decision, the duty cycle of the DC–DC boost converter is updated, and PWM pulses are generated to control the converter switch. By continuously adjusting the duty cycle, the P&O MPPT algorithm forces the PV array to operate close to its maximum power point, thereby improving solar energy utilization, maintaining a stable DC-link voltage, and increasing the overall efficiency of the proposed solar PV-assisted EV charging system.

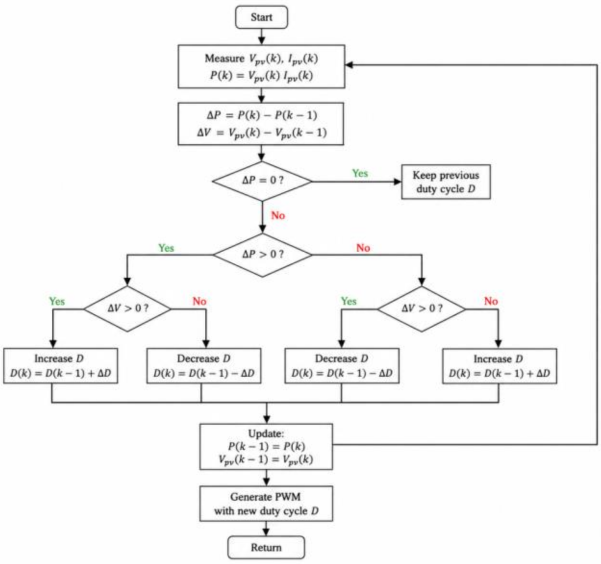

Fig. 4. Flowchart of the P&O MPPT Algorithm

IV. Bidirectional DC–DC Zeta Converter

The proposed bidirectional DC–DC Zeta converter serves as the interface between the DC-link and the electric vehicle (EV) battery. It enables bidirectional power transfer during both Grid-to-Vehicle (G2V) and Vehicle-to-Grid (V2G) operating modes while maintaining continuous input and output currents as shown in Fig.5. Compared with conventional buck–boost converters, the Zeta converter provides reduced current ripple, lower switching losses, higher conversion efficiency, and improved dynamic response, making it suitable for EV charging applications. During the charging mode (G2V), electrical energy is transferred from the DC-link to the EV battery. The switches Sev1 and Sev2are controlled complementarily to regulate the battery charging current. The inductors Lev1 and Lev2 store and transfer energy through the coupling capacitor Cev1, while the output capacitor Cev2 maintains a stable battery voltage. The discharging mode (V2G), the converter operates in reverse power flow. The energy stored in the EV battery is transferred back to the DC-link through the same converter, thereby supporting the utility grid during peak demand. The bidirectional operation ensures smooth transition between charging and discharging while maintaining regulated DC-link voltage and battery current.

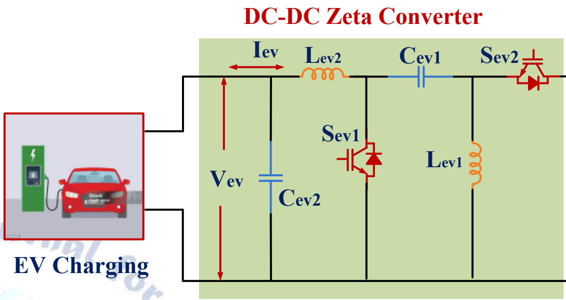

Fig. 5. Bidirectional DC–DC Zeta Converter for EV Battery Charging

A. Mathematical Model

Applying Kirchhoff's Voltage Law (KVL) to the converter gives

Inductor Lev1

$$L_{ev1}\frac{di_{L_1}}{dt} = V_{dC} - V_{C_1}(1-D) \quad (15)$$

Inductor Lev2

$$L_{ev_2}\frac{di_{L_2}}{dt} = V_{C1} - V_{ev} \quad (16)$$

Where V_{dc} = DC-link voltage, V_{ev} = EV battery voltage, V_{c1} = Coupling capacitor voltage, D = Duty cycle

Applying Kirchhoff's Current Law (KCL)

Coupling Capacitor

$$C_{ev_1}\frac{dV_{C_1}}{dt} = i_{L_1} - (1-D) \quad (17)$$

Output Capacitor

$$C_{ev_2}\frac{dV_{ev}}{dt} = i_{L_2} - \frac{V_{ev}}{R} \quad (18)$$

where

R represents the equivalent battery load.

B. Voltage Conversion Ratio

For continuous conduction mode (CCM), the voltage gain of the bidirectional Zeta converter is

$$\frac{V_{ev}}{V_{dC}} = \frac{D}{1-D} \quad (19)$$

The output battery voltage is therefore

$$V_{ev} = \frac{D}{1-D}V_{dc} \quad (20)$$

C. State-Space Model

The state variables are selected as

$$x_1 = i_{L_1}$$
$$x_2 = i_{L_2}$$
$$x_3 = V_{c_1} \quad (21)$$
$$x_4 = V_{ev}$$

The state vector is

$$x = \begin{bmatrix} i_{L1} \\ i_{L_2} \\ V_{c1} \\ V_{ev} \end{bmatrix} \quad (22)$$

The averaged state equations are

$$\frac{di_{L_1}}{dt} = \frac{V_{dc}-(1-D)V_{C_1}}{L_{ev_1}} \quad (23)$$

$$\frac{di_{L_2}}{dt} = \frac{V_{C_1}-V_{ev}}{L_{ev_2}} \quad (24)$$

$$\frac{dV_{C_1}}{dt} = \frac{i_{L_1}-(1-D)i_{L_2}}{C_{ev_1}} \quad (25)$$

$$\frac{dV_{ev}}{dt} = \frac{i_{L_2}}{C_{ev_2}} - \frac{V_{ev}}{RC_{ev_2}} \quad (26)$$

D. State-Space Representation

The dynamic model can be written as

$$\dot{x} = Ax + Bu \quad (27)$$

Where

$$u = V_{dc} \quad (28)$$

and

$$A = \begin{bmatrix} 0 & 0 & -\frac{1-D}{L_{ev_1}} & 0 \\ 0 & 0 & \frac{1}{L_{ev_2}} & -\frac{1}{L_{ev_2}} \\ \frac{1}{C_{ev_1}} & -\frac{1-D}{C_{ev_1}} & 0 & 0 \\ 0 & \frac{1}{C_{ev_2}} & 0 & -\frac{1}{RC_{ev_2}} \end{bmatrix} \quad (29)$$

$$B = \begin{bmatrix} \frac{1}{L_{ev_1}} \\ 0 \\ 0 \\ 0 \end{bmatrix} \quad (30)$$

V. THREE-PHASE AC–DC CONVERTER

The proposed three-phase AC–DC Voltage Source Converter (VSC) interfaces the utility grid with the common DC-link of the solar PV-assisted bidirectional EV charging station. Its primary objective is to regulate the DC-link voltage, control active and reactive power exchange, maintain unity power factor, and provide a stable DC supply for the bidirectional Zeta converter. An LCL filter is connected between the utility grid and the VSC to suppress switching harmonics and improve the quality of the injected grid current. The converter is controlled using an Adaptive Artificial Neural Network (ANN)-based Model Predictive Controller (MPC). The grid voltages are synchronized through a Phase-Locked Loop (PLL), and the measured three-phase voltages and currents are transformed into the synchronous rotating dq reference frame using the Park transformation. The ANN generates the optimal reference current based on the DC-link voltage error, while the MPC predicts the future converter states and selects the optimal switching state that minimizes the control cost function. Consequently, the converter maintains a constant DC-link voltage, fast transient response, and improved power quality during both Grid-to-Vehicle (G2V) and Vehicle-to-Grid (V2G) operating modes.

A. Mathematical Model in dq Reference Frame

The three-phase converter dynamics are represented in the synchronous dq reference frame as

$$L_f \frac{di_d}{dt} = V_d - V_{cd} + \omega L_f iq \quad (31)$$

$$L_f \frac{diq}{dt} = V_q - V_{cq} - \omega L_f i_d \quad (32)$$

Where V_d, Vq = Grid voltages, V_{Cd}, V_{Cq} = Converter voltages, i_d, iq = Gride Currents, L_f = Filter Inductance, ω = Grid angular frequency

B. DC-Link Voltage Dynamics

The DC-link capacitor stores the energy exchanged between the AC and DC sides.

Applying Kirchhoff's Current Law,

$$C_{dc}\frac{dV_{dc}}{dt} = I_{dc} - I_L \quad (33)$$

Where C_{dc} = DC-link capacitance, I_{dc} = Converter current, I_L = Load current

The DC-Link energy is

$$E = \frac{1}{2} C_{dc} V_{dc}^2 \quad (34)$$

C. Active and Reactive Power

The converter regulates both active and reactive power according to

$$P = \frac{3}{2}\left(V_d i_d + V_q i_q\right) \quad (35)$$

$$Q = \frac{3}{2}\left(V_q i_d - V_d iq\right) \quad (36)$$

For unity power factor,

$$i_q^{ref} = 0 \quad (37)$$

D. State-Space Model

The state variables are selected as

$$x_1 = i_d \tag{38}$$

$$x_2 = i_q \tag{39}$$

$$x_3 = V_{dc} \tag{40}$$

The state vector is

$$x = \begin{bmatrix} i_d \\ i_q \\ V_{dc} \end{bmatrix} \tag{41}$$

The state equations become

$$\frac{di_d}{dt} = \frac{V_d - V_{cd} + \omega L_f i_q}{L_f} \tag{42}$$

$$\frac{di_q}{dt} = \frac{V_q - V_{cq} - \omega L_f i_d}{L_f} \tag{43}$$

$$\frac{dV_{dc}}{dt} = \frac{I_{dc} - I_L}{C_{dc}} \tag{44}$$

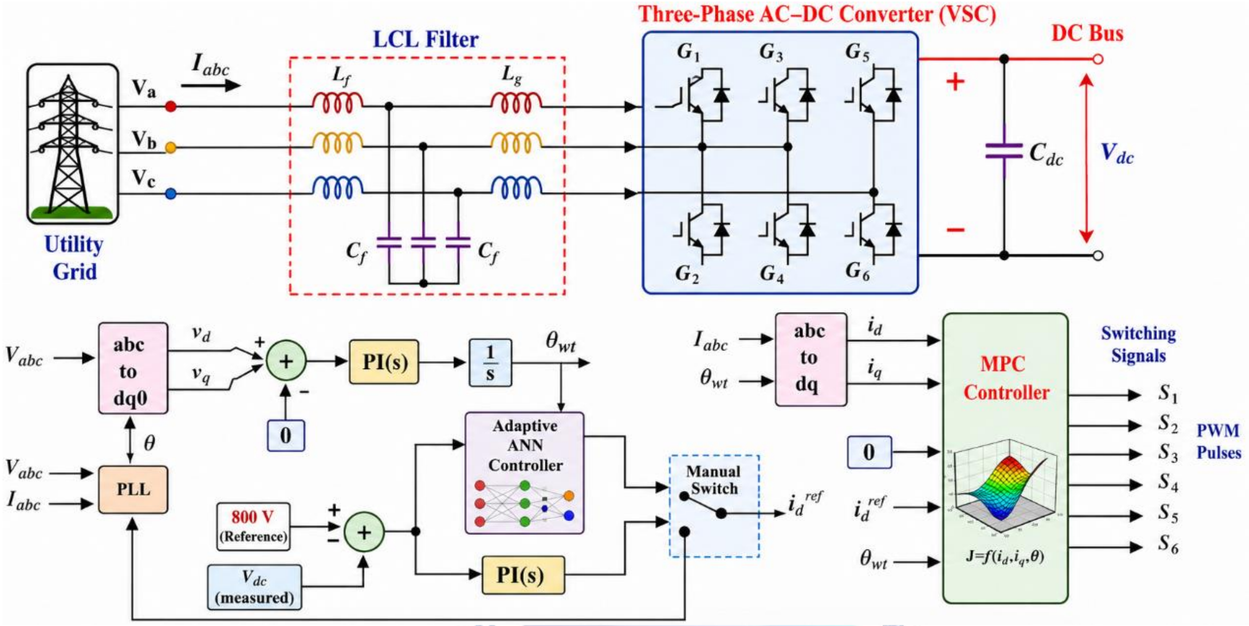

Fig. 6. Adaptive ANN–MPC Control Scheme for the Three-Phase AC–DC Voltage Source Converter (VSC)

VI. ADAPTIVE ARTIFICIAL NEURAL NETWORK (ANN) CONTROLLER

The proposed system employs an Adaptive Artificial Neural Network (ANN) controller to improve the dynamic performance of the grid-side converter and provide accurate reference current generation under varying operating conditions. Unlike conventional PI controllers, the ANN controller possesses self-learning and adaptive capabilities, enabling it to effectively handle nonlinearities, parameter uncertainties, and rapid changes in solar irradiance, load demand, and bidirectional power flow. The ANN continuously adjusts the control action based on the DC-link voltage error, thereby enhancing voltage regulation, reducing steady-state error, and improving transient response. The ANN consists of an input layer, a hidden layer, and an output layer. The input layer receives the DC-link voltage error and the change in voltage error, while the hidden layer processes the information using nonlinear activation functions. The output layer generates the reference direct-axis current i_d^{ref}, which is supplied to the Model Predictive Controller (MPC) for optimal switching state selection.

A. ANN Input Variables

The input error is defined as

$$e(k) = V_{dc}^{ref} - V_{dc}(k) \tag{45}$$

The change in error is

$$\Delta e(k) = e(k) - e(k-1) \tag{46}$$

The ANN input vector is

$$X(k) = \begin{bmatrix} e(k) \\ \Delta e(k) \end{bmatrix} \tag{47}$$

B. Hidden Layer Output

The weighted input to the hidden neuron is

$$z_j = \sum_{i=1}^{n} W_{ij} X_i + b_j \tag{48}$$

where

- W_{ij} = Weight between input and hidden neurons
- b_j = Hidden layer bias

The hidden neuron output is obtained using the sigmoid activation function

$$H_j = \frac{1}{1+e^{-z_j}} \tag{49}$$

C. Output Layer

The ANN output is

$$y = \sum_{j=1}^{m} V_j H_j + b_0 \tag{50}$$

where

- V_j = Hidden-to-output weights
- b_0 = Output bias

The generated output corresponds to the reference direct-axis current

$$i_d^{ref} = y \tag{51}$$

D. Weight Update Equation

The ANN weights are updated using the gradient descent learning rule

$$W_{ij}(k+1) = W_{ij}(k) + \eta \delta_j X_i \tag{52}$$

where

- η = Learning rate
- δ_j = Error signal

The output error is

$$E = \frac{1}{2}\left(i_d^{ref} - i_d\right)^2 \tag{53}$$

The objective of the ANN is to minimize this error continuously.

E. ANN Control Output

The reference current generated by the ANN is supplied to the MPC controller as

$$i_d^{ref} = ANN(e, \Delta e) \tag{54}$$

The reactive current reference is maintained as

$$i_q^{ref} = 0 \tag{55}$$

to achieve unity power factor operation.

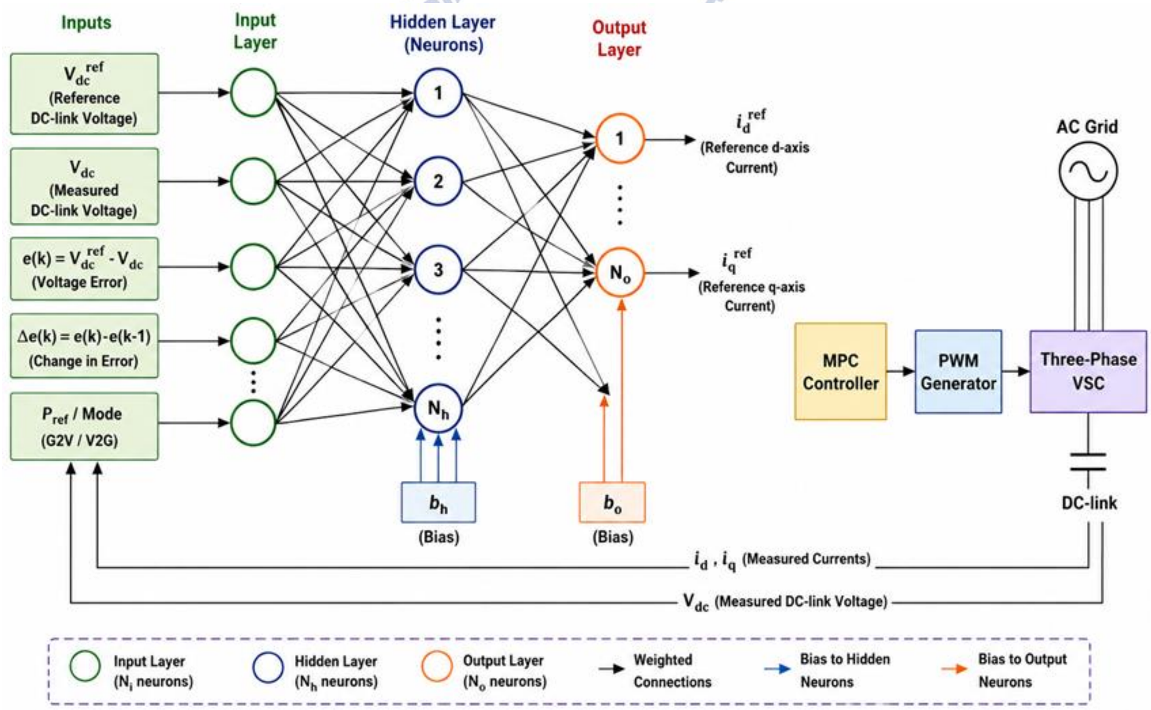

Fig. 7. Proposed Adaptive ANN Controller Structure for the Grid-Side AC–DC Converter

VII. MODEL PREDICTIVE CONTROLLER (MPC)

The proposed control strategy employs a Finite Control Set Model Predictive Controller (FCS-MPC) to regulate the three-phase Voltage Source Converter (VSC). Unlike conventional PI controllers, the MPC predicts the future converter currents for all possible switching states and selects the switching state that minimizes a predefined cost function. This approach provides fast dynamic response, excellent current tracking capability, reduced steady-state error, and improved power quality during both Grid-to-Vehicle (G2V) and Vehicle-to-Grid (V2G) operating modes.

At every sampling instant, the converter has eight possible switching states

$$s = \begin{bmatrix} 0 & 0 & 0 \\ 0 & 0 & 1 \\ 0 & 1 & 0 \\ 0 & 1 & 1 \\ 1 & 0 & 0 \\ 1 & 0 & 1 \\ 1 & 1 & 0 \\ 1 & 1 & 1 \end{bmatrix} \quad (56)$$

Where

$$S = [S_a, S_b, S_c] \quad (57)$$

And

$$S_a, S_b, S_c \in \{0,1\} \quad (58)$$

represent the switching states of the three converter legs.

A. Converter Output Voltage

The phase voltages generated by the converter are

$$Va = \frac{V_{dc}}{3}(2S_a - S_b - S_c) \quad (59)$$

$$V_b = \frac{V_{dc}}{3}(2S_b - S_a - S_c) \quad (60)$$

$$V_c = \frac{V_{dc}}{3}(2S_c - S_a - S_b) \quad (61)$$

Where

- V_{dc} = DC-link voltage.

B. Park Transformation

The converter voltages are transformed into the synchronous rotating dq reference frame using the Park transformation.

The q-axis voltage is

$$V_q = \frac{2}{3}[V_a \cos\theta + V_b \cos\left(\theta - \frac{2\pi}{3}\right) + V_c \cos\left(\theta + \frac{2\pi}{3}\right)] \quad (62)$$

Similarly, the d-axis voltage is

$$V_d = \frac{2}{3}\left[V_a \sin\theta + V_b \sin\left(\theta - \frac{2\pi}{3}\right) + V_c \sin\left(\theta + \frac{2\pi}{3}\right)\right] \quad (63)$$

Where

θ is obtained from the Phase locked loop (PLL).

C. Current Prediction Model

Using the discrete-time forward Euler approximation, the predicted d-axis current is

$$i_d(k+1) = \left(1 - \frac{RT_s}{L}\right) i_d(k) + T_s i_q(k) + \frac{T_s}{L} V_d \quad (64)$$

Similarly, the predicted q-axis current becomes

$$i_q(k+1) = \left(1 - \frac{RT_s}{L}\right) i_q(k) - T_s i_d(k) + \frac{T_s}{L} V_q \quad (65)$$

where

- Ts= Sampling period
- L = Filter inductance
- R = Filter resistance

These equations estimate the converter currents corresponding to each possible switching

Cost Function

The MPC evaluates the predicted currents using the quadratic cost function

$$J = \left(i_d^{ref} - i_d(k+1)\right)^2 + \left(i_q^{ref} - i_q(k+1)\right)^2 \quad (66)$$

Where

- $i_d^{ref} = Refrence\ d - axis\ current$
- $i_q^{ref} = Reference\ q - axis\ current$

The objective of the controller is to minimize the cost function

$$\bar{J} = min(\bar{J_i}) \quad (67)$$

for all eight switching vectors.

Optimal Switching Selection

The optimal switching state is obtained as

$$S_{opt} = arg\,min\{J_i, J_2, \ldots, J_8\} \quad (68)$$

The selected switching vector generates the PWM pulses for the converter switches

$$Pulse = [S_1, S_2, S_3, S_4, S_5, S_6] \quad (69)$$

Which are applied to the three-phase VSC.

VIII. SIMULATION RESULTS AND DISCUSSION

The proposed Adaptive Artificial Neural Network (ANN)-based Model Predictive Control (MPC) strategy for the solar PV-connected bidirectional EV charging station was developed and validated in the MATLAB/Simulink environment. The system performance was evaluated under different operating conditions, including Grid-to-Vehicle (G2V) charging, Vehicle-to-Grid (V2G) discharging, and sudden power variations. The effectiveness of the proposed controller was investigated by analyzing grid voltage, grid current, active power, grid frequency, DC-link voltage, photovoltaic output characteristics, battery voltage, battery current, and battery state of charge (SOC). The obtained results were also compared with the conventional PI controller to demonstrate the superiority of the proposed ANN-MPC approach.

A. Grid Performance

Fig.8 illustrates the grid-side performance of the proposed solar PV-assisted bidirectional EV charging station under the conventional PI and proposed Adaptive ANN controllers. The three-phase grid voltage remains balanced with peak amplitude of approximately ±340 V under both controllers, indicating proper synchronization with the utility grid. The grid current is regulated within ±50 A, where the proposed ANN controller exhibits smoother current waveforms and reduced oscillations compared with the PI controller during G2V and V2G transitions. The active power varies between −20 kW and +13 kW; however, the ANN controller achieves faster stabilization with lower overshoot, whereas the PI controller exhibits comparatively larger transient oscillations. Similarly, the grid frequency is maintained close to 50 Hz, varying between 49.995–50.012 Hz for the PI controller and 49.998–50.008 Hz for the proposed ANN controller, demonstrating improved frequency regulation. The DC-link voltage is regulated around 800 V, where the PI controller exhibits an overshoot of approximately 845 V and an undershoot of 780 V, while the proposed ANN controller limits the voltage variation to approximately 842 V and 790 V, respectively. These results confirm that the proposed Adaptive ANN controller provides improved dynamic performance, reduced oscillations, enhanced voltage regulation, and superior grid stability compared with the conventional PI controller.

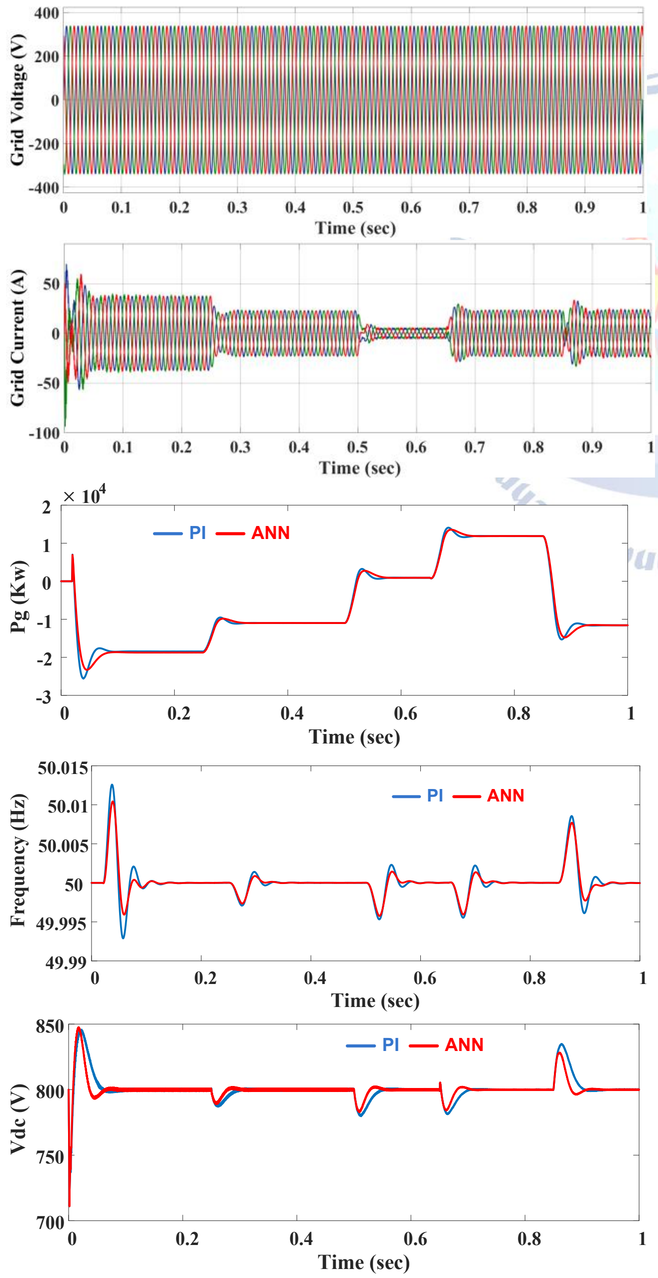

Fig. 8. Grid-Side Performance of the Proposed Adaptive ANN–MPC Controlled Bidirectional EV Charging Station.

B. Solar PV Performance

Fig.9 illustrates the performance of the solar PV system under varying operating conditions. The PV voltage Vpv is maintained at approximately 300 V during normal operation and gradually decreases to about 120 V as the solar irradiance reduces. Similarly, the PV current Ipv initially reaches approximately 100 A, decreases to 75 A, then 40 A, and finally approaches 0 A as the available solar energy diminishes. Consequently, the PV output power Ppv varies from approximately 30 kW to 20 kW, then 10 kW, and finally 0 kW, following the changes in irradiance. The P&O MPPT algorithm continuously tracks the maximum power point and regulates the DC–DC boost converter to maximize energy extraction under all operating conditions. These results demonstrate stable photovoltaic operation, effective maximum power point tracking, and efficient utilization of available solar energy in the proposed EV charging station.

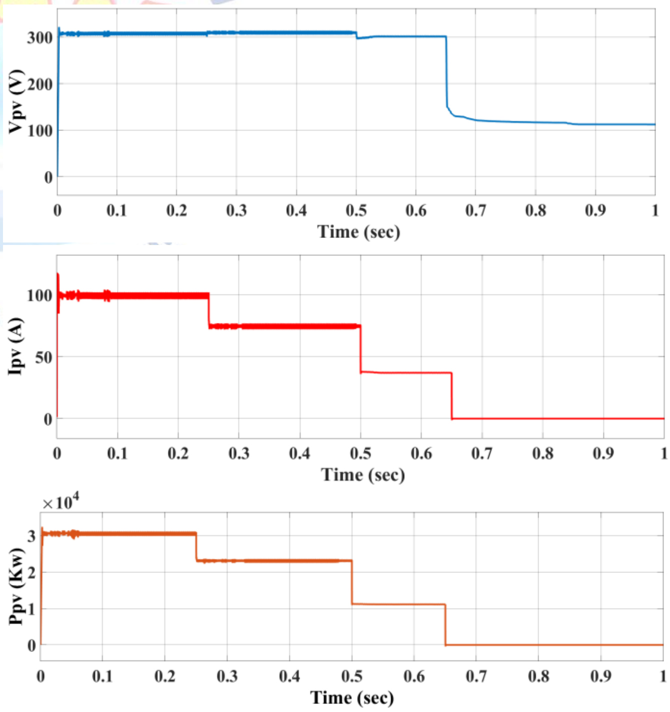

Fig. 9 Solar PV Output Performance of the Proposed Adaptive ANN–MPC Controlled EV Charging System.

C. EV Battery Performance

Fig.10 illustrates the performance of the EV battery during charging and discharging operations. The battery voltage Vb is maintained at approximately 390 V throughout the simulation, indicating stable voltage regulation by the bidirectional Zeta converter. The battery current Ib initially reaches approximately 100 A during the transient period and then stabilizes around −30 A during charging. At approximately 0.85 s, the current changes to about +30 A, indicating the transition from Grid-to-Vehicle (G2V) charging to Vehicle-to-Grid (V2G) discharging operation. Furthermore, the battery State of Charge (SOC) gradually increases from approximately 50.368% to 50.3705% during the charging interval, confirming efficient energy transfer and effective battery management. These results demonstrate stable battery voltage, smooth bidirectional current regulation, and reliable charging/discharging performance, validating the effectiveness of the proposed Adaptive ANN–MPC controlled bidirectional EV charging station.

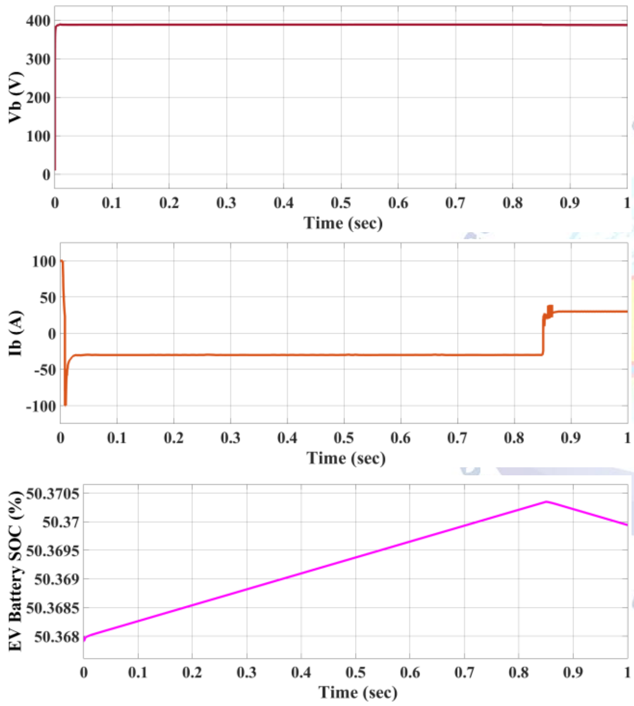

Fig. 10. EV Battery Output Performance of the Proposed Adaptive ANN–MPC Controlled EV Charging System.

D. Total Harmonic Distortion (THD) Analysis

Fig. 11 shows the FFT analysis of the grid current for the conventional PI controller and the proposed Adaptive ANN controller. The PI controller achieves a THD of 4.75% at the fundamental frequency of 50 Hz, whereas the proposed Adaptive ANN controller reduces the THD to 2.49%. This significant reduction in harmonic distortion demonstrates the superior current regulation capability of the proposed controller, resulting in improved power quality and smoother converter operation. Moreover, the obtained THD value is well within the IEEE 519 limit of 5%, confirming the effectiveness of the proposed controller for grid-connected EV charging applications.

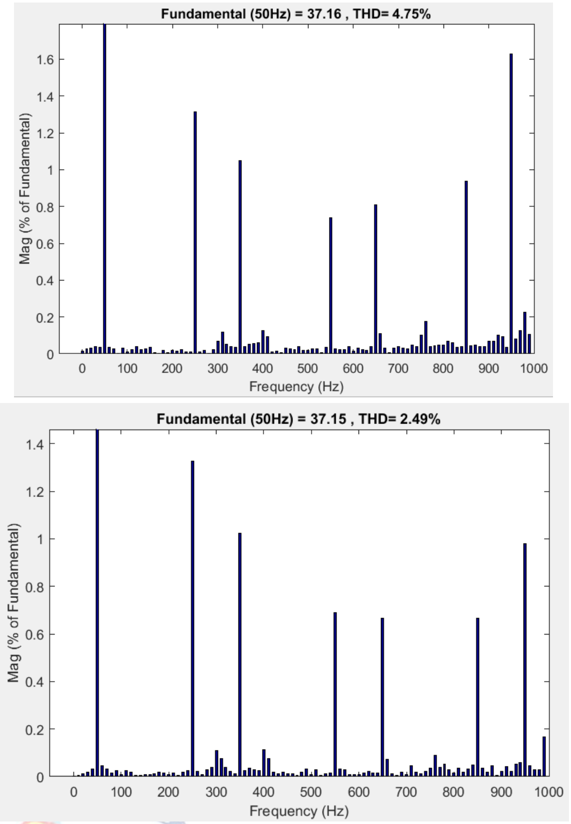

Fig. 11 FFT Analysis of Grid Current THD Using the Conventional PI Controller and the Proposed Adaptive ANN Controller.

XI CONCLUSION

This paper presented an Adaptive Artificial Neural Network (ANN)-based Model Predictive Control (MPC) strategy for a solar PV-assisted bidirectional EV charging station employing a bidirectional DC–DC Zeta converter. The proposed controller effectively regulated the DC-link voltage, controlled bidirectional power flow during G2V and V2G operations, and enhanced grid stability under varying operating conditions. The integration of the P&O MPPT algorithm enabled efficient solar energy utilization, while the bidirectional Zeta converter ensured high conversion efficiency and smooth battery charging/discharging. Simulation results obtained in MATLAB/Simulink demonstrated improved transient response, reduced voltage and current oscillations, enhanced power quality, and stable grid frequency compared with conventional control methods. Furthermore, the proposed system maintained THD within IEEE 519 limits, confirming its effectiveness as a reliable and intelligent control solution for next-generation grid-connected solar PV-assisted bidirectional EV charging stations.

Conflict of interest statement

Authors declare that they do not have any conflict of interest.

REFERENCES

[1] M. Yilmaz and P. T. Krein, "Review of Battery Charger Topologies, Charging Power Levels, and Infrastructure for Plug-In Electric and Hybrid Vehicles," IEEE Transactions on Power Electronics, vol. 28, no. 5, pp. 2151–2169, May 2013.

[2] S. Habib, M. Kamran, and U. Rashid, "Impact Analysis of Vehicle-to-Grid Technology and Charging Strategies of Electric Vehicles on Distribution Networks," Journal of Power Sources, vol. 277, pp. 205–214, 2015.

[3] W. Kempton and J. Tomic, "Vehicle-to-Grid Power Fundamentals: Calculating Capacity and Net Revenue," Journal of Power Sources, vol. 144, no. 1, pp. 268–279, Jun. 2005.

[4] C. C. Chan, "The State of the Art of Electric, Hybrid, and Fuel Cell Vehicles," Proceedings of the IEEE, vol. 95, no. 4, pp. 704–718, Apr. 2007.

[5] S. M. Arif, T. T. Lie, B. C. Seet, S. Ayyadi, and K. Jensen, "Review of Electric Vehicle Technologies, Charging Methods, Standards and Optimization Techniques," Electronics, vol. 10, no. 16, 2021.

[6] M. Parvez, S. Mekhilef, N. M. L. Tan, and H. Akagi, "Model Predictive Control of a Bidirectional AC–DC Converter for V2G and G2V Applications in Electric Vehicle Battery Charger," IEEE Conference Proceedings, 2014.

[7] S. Mekhilef, M. Parvez, and H. Akagi, "Bidirectional AC–DC Converter Control for Electric Vehicle Applications," IEEE Transactions on Industrial Electronics, 2015.

[8] X. Tang, C. Sun, S. Bi, S. Wang, and A. Y. Zhang, "A Holistic Review on Advanced Bi-directional EV Charging Control Algorithms," 2022.

[9] M. A. Hannan, M. M. Hoque, A. Mohamed, and A. Ayob, "Review of Energy Storage Systems for Electric Vehicle Applications," Renewable and Sustainable Energy Reviews, vol. 69, pp. 771–789, 2017.

[10] M. Ehsani, Y. Gao, and A. Emadi, Modern Electric, Hybrid Electric and Fuel Cell Vehicles, 3rd ed., CRC Press, 2018.

[11] IEEE Standard 519-2022, IEEE Recommended Practice and Requirements for Harmonic Control in Electric Power Systems, IEEE, 2022.

[12] IEEE Standard 1547-2018, IEEE Standard for Interconnection and Interoperability of Distributed Energy Resources with Associated Electric Power Systems Interfaces, IEEE, 2018.

[13] M. H. Rashid, Power Electronics: Circuits, Devices and Applications, 4th ed., Pearson, 2014.

[14] R. W. Erickson and D. Maksimovic, Fundamentals of Power Electronics, 3rd ed., Springer, 2020.

[15] S. Mamidala and Y. V. Pavan Kumar, "Zeta Converter Integration for Improved Power Quality in Bidirectional V2G Energy Charging Stations," Results in Engineering, vol. 28, 2025.

[16] S. Mamidala and Y. V. Pavan Kumar, "Closed Loop Battery Current Controlled Zeta Converter for Improved Power Quality in Electric Vehicle Charging Stations," 2024.

[17] M. P. Kazmierkowski and L. Malesani, "Current Control Techniques for Three-Phase Voltage Source PWM Converters," IEEE Transactions on Industrial Electronics, vol. 45, no. 5, pp. 691–703, Oct. 1998.

[18] J. Rodriguez, M. P. Kazmierkowski, J. R. Espinoza, et al., "State of the Art of Finite Control Set Model Predictive Control in Power Electronics," IEEE Transactions on Industrial Informatics, vol. 9, no. 2, pp. 1003–1016, May 2013.

[19] J. Rodriguez and P. Cortes, Predictive Control of Power Converters and Electrical Drives, Wiley-IEEE Press, 2012.

[20] S. Kouro, P. Cortes, R. Vargas, U. Ammann, and J. Rodriguez, "Model Predictive Control—A Simple and Powerful Method to Control Power Converters," IEEE Transactions on Industrial Electronics, vol. 56, no. 6, pp. 1826–1838, Jun. 2009.

[21] B. Ejaz, R. Zamora, C. Reusser, and X. Lin, "A Comprehensive Review of Partial Power Converter Topologies and Control Methods for Fast Electric Vehicle Charging Applications," Electronics, vol. 14, no. 10, 2025.

[22] D. Jaraniya et al., "Multifunctional Bidirectional Charging System for EVs and Grid Support," CSEE Journal of Power and Energy Systems, vol. 9, no. 5, pp. 1753–1765, 2023.

[23] A. Emadi, K. Rajashekara, S. Williamson, and S. Lukic, "Topological Overview of Hybrid Electric and Fuel Cell Vehicular Power System Architectures," IEEE Transactions on Vehicular Technology, vol. 54, no. 3, pp. 763–770, May 2005.

[24] M. Brenna, F. Foiadelli, and D. Zaninelli, Electric Vehicle Charging Technology for Smart Grids, Springer, 2020.

[25] M. Safayatullah, M. T. Elrais, S. Ghosh, R. Rezaii, and I. Batarseh, "A Comprehensive Review of Power Converter Topologies and Control Methods for Electric Vehicle Fast Charging Applications," IEEE Access, vol. 10, pp. 40753–40793, 2022.